Elastohydrodynamics of a Moving Substrate Over a Curved Plate

M. S. Carvalho, G. L. Huelsman, and W. B. Kolb
Imation Corporation, Oakdale, MN, 55128

Conventional drying of coated substrates usually uses air impingement to support and heat the coated web. Because of the high-velocity air flow, most of the heat is transferred by convection and the heat transfer coefficient is not uniform, leading to drying defects. To overcome this and obtain a high uniform heat transfer coefficient, the energy is supplied to the backside of the substrate by conduction through a thin air-layer between a heated plate and the moving substrate. To obtain heat transfer coefficients comparable to those from air impingement, the distance between the web and plate has to be very small, yet not touch the plate. It is essential to form and control a thin, uniform and stable air layer between the substrate and heating plate by wrapping the moving web over a plate with a large radius of curvature. Air-layer thickness entrained between the web and plate is related to the air flow rate between the two surfaces. The flow between a moving flexible substrate and curved solid surface was analyzed by theory and experiments to examine this elastohydrodynamic action and changes in air-layer thickness with the plate geometry, substrate material, and operating conditions. The theoretical model consisted of the Navier–Stokes equation to describe the air motion and cylindrical shell approximation to model the web deformation. Differential equations describing the problem were solved by the Galerkin's/finite-element method. The nonlinear algebraic system was solved by Newton's method with initialization by pseudo-arc-length continuation. In experiments, the distance between the moving web and curved plate was measured at different operating conditions. The predicted air-layer thicknesses agreed well with experimental measurements. The air-layer thickness is controlled by the flow in the plate entrance.

Introduction

When a flexible moving substrate is traveling over a solid surface, a thin layer of air is entrapped between the two surfaces. This case of hydrodynamic lubrication is generally referred to as foil bearing.

The control of the thickness of the air layer between the surfaces is vital in many situations. When a roll of film is formed, an optimum air thickness between each layer of film together with the film roughness controls the amount of film-to-film contact. The air acts as a lubricant. If the amount of air entrapped is large, there is not enough surface contact, the layers ride on air, and can move in the transverse direction, causing a failure of the roll-formation process. If the air-layer thickness is small, the film-to-film contact is large and tension is not well transmitted (see Knox and Sweeney, 1971). Another important situation is when a magnetic tape is traveling over a read–write head. The signal loss is proportional to the separation between the tape and the head (see Eshel, 1970). The application that motivated this work is related to the floatation of a moving substrate over hot solid surfaces inside an oven, as described next.

Drying of coated substrate

The conventional drying process for coated substrates usually uses impingement dryer technology, as sketched in Figure 1. Nozzles of varying design impinge air to the web. Air serves to support the web, and to supply heat to the coated

Correspondence concerning this article should be addressed to M. S. Carvalho at this current address: Dept. of Mechanical Engineering, Pontifícia Universidade Católica do Rio de Janeiro (PUC-Rio), Rua Marques de São Vicente, 225, Gávea, Rio de Janerio, 22453-900, RJ, Brazil.

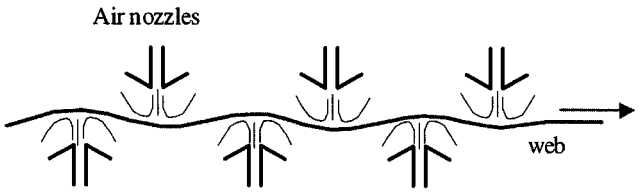

Figure 1. Impingement dryer.

substrate. With this technology, the need for idlers and driven rolls inside the oven is eliminated and the coating quality is improved by avoiding scratches caused by contact between the substrate and the rolls. Because of the high-velocity air flow, most of the heat is transferred to the web by convection. The air flow is highly nonuniform, leading to nonuniform heat-transfer coefficient: it is large in the region close to the nozzle and low far from the nozzle, where the air velocity is low. This nonuniformity may lead to drying defects. Controlling the amount of energy supplied to the web is not easy. The air flow is turbulent and complex. The effect of the operating parameters on the drying rate is usually determined after extensive trial-and-error experimentation. Moreover, the amount of air that needs to be treated for solvent-recovery purposes and pollution control is usually large.

A new drying technology, call *gap drying*, has been developed recently by Huelsman and Kolb (1997). This technology provides accurate control of heat- and mass-transfer rates, eliminates the need for forced gas flow, as in the case of impingement ovens, and provides direct solvent recovery. Kolb and Hueslman (1998) discuss the advantages of this new drying method when compared to existing methods.

In a gap dryer, heat to evaporate the solvent is supplied to the substrate from the back side, and a chilled plate is located above the web to remove the solvent by condensation, as illustrated in Figure 2. The cold plate is provided with a surface geometry that prevents the liquid from dripping back onto the coated surface and "pumps" the condensed solvent off the plate into a collection device.

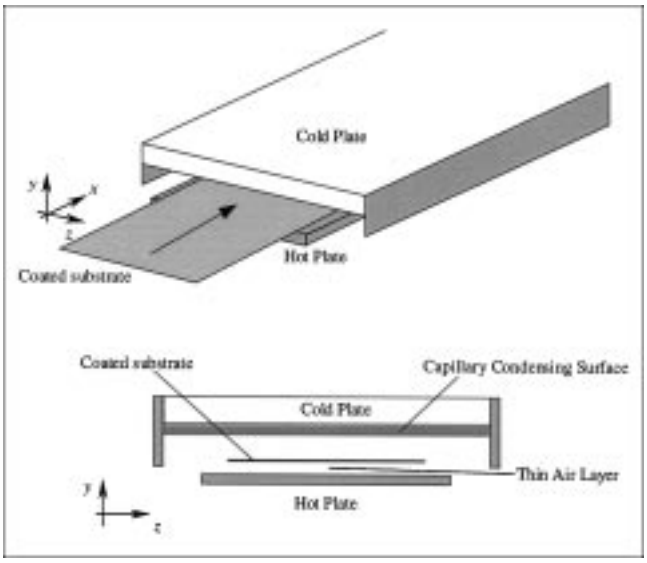

Figure 2. Gap dryer with cross section perpendicular to direction of web motion.

The energy is transferred from the hot plate to the backside of the substrate mainly by conduction through the air layer between the two surfaces. Therefore, the heat-transfer coefficient is given by the ratio of thermal conductivity of air to the air-layer thickness. To obtain large, comparable with those obtained by conventional air impingement dryers, and uniform heat-transfer coefficients, the air-layer thickness has to be very small and constant in both time and space.

A uniform, stable, and thin air layer between a moving substrate and a heated plate without forced air can be obtained by using a plate with a large radius of curvature, positioned such that the web wraps part of it, as indicated in Figure 3. The moving web drags air, and a thin layer of air under pressure is formed between the web and the plate. The amount of air entrapped between the two surfaces is controlled by the plate geometry, web speed, and substrate tension.

The goal of this work is to understand how the air film thickness changes with the geometry of the plate and operating conditions. This information is used to design plates such that the air thickness can be adjusted according to the drying rates required by different products.

Foil bearing

The first analysis of foil bearing was done by Blok and Van Rossum (1953). They measured the thickness of a lubricating oil layer between a thin cellophane foil and a cylinder. Using a simplified analysis, they derived an expression for the oil thickness H_0

$$H_0 = 0.426 R_0 \left(6 \frac{\mu V}{T}\right)^{2/3} \tag{1}$$

where R_0 is the cylinder radius, μ is the fluid viscosity, V is the web speed, and T the tension of the web.

Eshel and Elrod (1965) developed a theoretical model using the Reynolds equation of lubrication to describe the fluid flow with the assumptions of fluid incompressibility, and infinitely wide foil of negligible stiffness. The relationship between the fluid thickness and operating parameters they de-

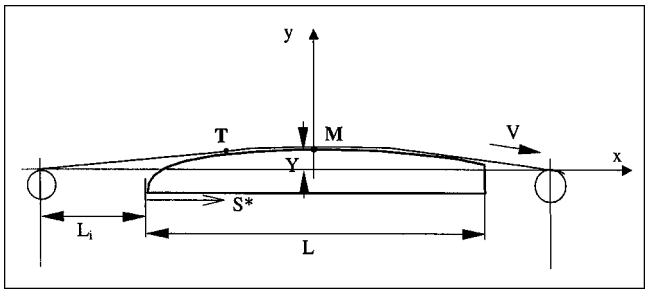

Figure 3. Geometry of a substrate moving over a curved plate.

The upstream and downstream idlers are positioned such that the web wraps part of the plate.

rived is

$$H_0 = 0.643R_0\left(6\frac{\mu V}{T}\right)^{2/3} \tag{2}$$

Eshel and Elrod later (1967) extended their work and analyzed the effect of foil stiffness. They showed that, for the range of parameters they explored, the stiffer the web, the smaller the air-layer thickness.

Licht (1968) presented an extensive experimental study of elastohydrodynamic lubrication of foil bearings. His measurements were in good agreement with the theoretical predictions of Eshel and Elrod.

Knox and Sweeney (1971) checked experimentally the validity of Eq. 2. They measured the coefficient of friction of film surfaces moving over cylinders under various conditions. Because of their experimental analysis and direct application to the roll formation process in the coating industry, the relation derived by Eshel and Elrod is also referred as the Knox–Sweeney equation.

All the works just mentioned analyzed the foil (web) traveling over a cylinder (or roll). However, the clearance predicted by Eq. 2 is much larger than the measured gap of a magnetic tape floating over a read–write head. Eshel (1970) used lubrication approximation to show qualitatively that the geometry of the head has a remarkable effect on the air film thickness. The later is sharply reduced by the corners in the solid over which the foil passes. In order to obtain an accurate relation between the air-layer thickness, the operating conditions, and plate configuration, a complete two-dimensional model for the air flow has to be employed.

In this work, the air motion is described by the Navier–Stokes equation, and the deformation of the substrate is modeled by the cylindrical shell approximation. The air flow and web deformation are assumed to be two-dimensional, that is, the flow and air thickness variation in the transverse direction are neglected. In reality, a small amount of air escapes from beneath the web through the sides. The differential equations that describe the problem are solved by the Galerkin/finite-element method. Experiments were performed in order to validate the accuracy of the theoretical model and to study the issues not accounted for in the model, such as air leakage through the sides and variation of the air-layer thickness in the transverse direction. The experiments consisted of measuring the distance between the moving web and the curved plate at different operating conditions and plate configurations. In general, the agreement between the predicted air-layer thickness and those measured experimentally at the center of the plate was very good.

Elastohydrodynamic Model

Governing equations

The configuration of the problem analyzed here is illustrated in Figure 3. The air dragged by the moving substrate (in the figure, the web is moving from left to right) generates pressure due to the converging channel formed between the substrate and the curved plate. The air pressure deforms the substrate. The flow and the deformation are coupled in what is called *elastohydrodynamic behavior*.

It is important to characterize the position of the plate relative to the upstream and downstream idler rolls that guide the moving web. For convenience, the x-coordinate axis is chosen to be the line that tangents both idlers, as illustrated in Figure 3. The position of the plate is characterized by the distance between the upstream idler and the front of the plate L_i and the distance Y from the middle point M of the plate to the x-axis. When $Y < 0$, the web does not touch the plate. When $Y > 0$, the web wraps around a portion of the plate. An alternative way of characterizing the relative position of the plate and idlers is by the distance from the point T, where the stationary web first touches the plate, to the upstream edge of the plate, denoted by S^* and shown in Figure 3. Each value of Y corresponds to one value of S^*. As the plate is pushed against the web and Y increases, the tangent point T moves toward the upstream edge of the plate, and S^* decreases.

The web is assumed to be infinitely wide, and therefore the flow in the transverse direction is neglected. The motion of the air is described by the Navier–Stokes equation and the continuity equation of incompressible Newtonian fluid

$$\rho \boldsymbol{v}\cdot\nabla\boldsymbol{v} - \nabla\cdot\left\{-p\mathbf{I} + \mu\left[\nabla\boldsymbol{v} + (\nabla\boldsymbol{v})^T\right]\right\} \text{ and } \nabla\cdot\boldsymbol{v} = 0 \tag{3}$$

together with appropriate boundary conditions. Here, ρ and μ are the air density and viscosity, respectively. The deformation of the web is modeled by the equations of cylindrical shells

$$\frac{dT}{d\xi} + \kappa\frac{d}{d\xi}(\kappa D) + P_t = 0$$

$$-\frac{d^2}{d\xi^2}(\kappa D) + \kappa T + P_n = 0$$

$$\frac{d^2x}{d\xi^2} + \kappa\frac{dy}{d\xi} = 0 \text{ or } \frac{d^2y}{d\xi^2} - \kappa\frac{dx}{d\xi} = 0 \tag{4}$$

where ξ is the coordinate along the web, T and κ are the web tension and curvature at each position, and x and y are the Cartesian coordinates of points on the web, as illustrated in Figure 4. The web stiffness $D \equiv Et^3/12(1-\nu^2)$ is a function of the Elastic Modulus E, Poisson ratio ν, and thickness

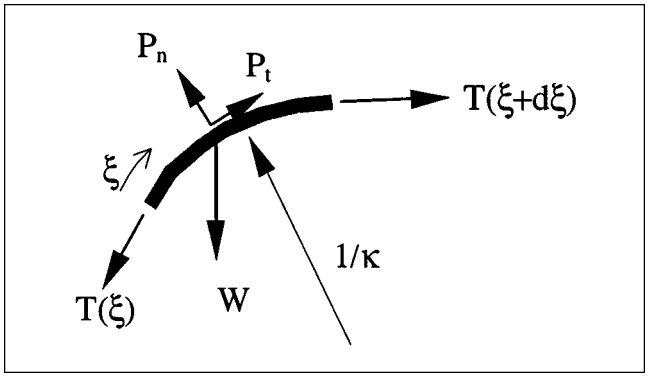

Figure 4. Forces acting on a substrate element.

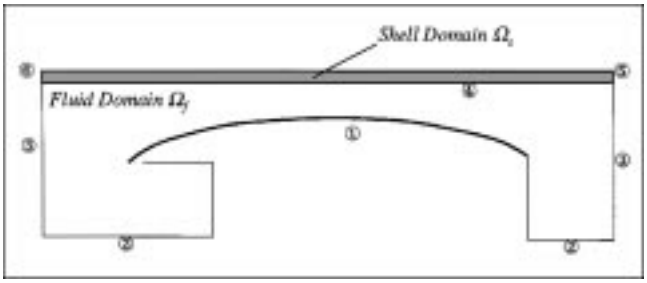

Figure 5. Domain of calculation.

Ω_f is the fluid domain, where the Navier–Stokes equation is solved, and Ω_s is the shell domain, where the cydindrical shell equations are solved.

of the web t; P_t and P_n are the loading forces on the web in the tangential and normal direction.

Figure 5 shows the domain of calculation. It is divided into two different subdomains: one where the Navier–Stokes equation is solved (Ω_f), and the other where the cylindrical shell equations are solved (Ω_s).

At the plate surface ①, the no-slip and no-penetration conditions apply, viz.

$$\boldsymbol{v} = 0 \tag{5a}$$

The artificial boundaries ② that limit the fluid domain underneath the plate were located far enough below the plate that its location had no effect on the predictions reported here. On that position, the air was assumed to be stagnant.

Along the artificial inflow and outflow boundary ③, the pressure is assumed constant (atmospheric pressure)

$$p = P_0 \tag{5b}$$

The inflow and outflow plane were positioned such that the theoretical predictions were virtually insensitive to moving the boundaries further away from the plate.

At the interface between the air and the flexible substrate ④, the air velocity is equal to the web velocity, viz.

$$\boldsymbol{v} = \boldsymbol{V}_{\mathbf{web}} \tag{5c}$$

and the loading force responsible for the web deformation is the traction exerted by the air. Underneath the web, the traction vector exerted by the air is

$$P_t = -\boldsymbol{t}\cdot(\boldsymbol{\sigma}\boldsymbol{n}) \text{ and } P_n = -\boldsymbol{n}\cdot(\boldsymbol{\sigma}\boldsymbol{n}) \tag{5d}$$

where $\boldsymbol{\sigma}$ is the Cauchy stress tensor, and $\boldsymbol{t}$ and $\boldsymbol{n}$ are the tangential and normal unitary vectors, respectively.

In one extreme of the substrate ⑤, the position, curvature, and web tension have to be specified

$$\boldsymbol{x} = \boldsymbol{X}_{\mathbf{up}};\ \kappa = 0; \text{ and } T = T_{\text{up}} \tag{5e}$$

In the other extreme ⑥, only the position and curvature are specified:

Table 1. Variables and Their Values for Gap Drying

Variable	Symbol	Range
Air density	ρ	10^{-3} g/cm^3
Air viscosity	μ	2×10^{-4} Poise
Web speed	V	20 to 1,000 ft/min
Web tension	T	0.5 to 5 lb/in.
Web thickness	t	0.5 to 7 mil
Web density	ρ_w	1.3 g/cm^3
Web elastic constant	$E/12(1-\nu^2)$	6×10^8 N/m^2
Position of the plate	Y	0 to 1.5 in.
Plate radius	R_0	40 to 120 ft
Plate length	L	2 to 10 ft
Free span from idler to plate	L_i	2.5 to 10 in.

$$\boldsymbol{x} = \boldsymbol{X}_{\mathbf{down}}; \text{and } \kappa = 0 \tag{5f}$$

The relevant variables for the situation of interest (gap drying) and their respective value ranges are listed in Table 1.

The revelant variables can be combined into the following dimensionless groups:

Reynolds number: $$Re \equiv \frac{\rho V H_0}{\mu}$$

Tension number: $$\tau \equiv \frac{\mu V}{T}$$

Elasticity number: $$Es \equiv \frac{D}{TR_0^2} = \frac{Et^3}{12(1-\nu^2)TR_0^2}$$

Weight number: $$W \equiv \frac{\rho_w g t L_i}{T}$$

Wrapping angle: $$\alpha \equiv \frac{L_s}{R_0}$$

Dimensionless length: $$\frac{L}{R_0}$$

The Reynolds number (Re) gives the ratio of inertial to viscous forces. The length scale used in its definition is the clearance between the web and the plate H_0. The Reynolds number for the flows explored here varied from 1 to 10. The Tension number characterizes the ratio between the viscous force (pressure) action on the web to the tension that is applied on it. For the cases explored here, it varies from 10^{-8} to 10^{-6}. The Elasticity number is the ratio between the moment required to bend the web to the radius of curvature of the plate to the moment of the tension about the center of the radius plate. Because the radius of curvature of the heated plates is large, the Elasticity numbers for the situation explored here are very small, on the order of 10^{-11}. The Weight number measures the amount of bending of the web on the free span between the upstream idler and the front edge of the plate. The Wrapping angle characterizes the relative position of the plate to the web; L_s is the length of the web that is in contact with the plate when the web speed is zero. It is directly related to the position of the plate Y or the position of the tangent point S^*.

The model presented here incorporates several simplifying assumptions. The first idealization is that the flow in the cross-web direction is neglected, that is, the flow is assumed

to be two-dimensional. In reality, because the air underneath the web is under pressure, a small amount of it escapes through the sides. The two-dimensional model also does not take into account the bagginess of the web. Another important simplification is that the mathematical formulation used to describe the situation enforces that there is always a layer of air between the web and the plate. Therefore, the theoretical calculations presented cannot predict at what conditions the web touches the plate. Nonetheless, this two-dimensional model can still capture the overall features and trends of the process. It clarifies how and why the air-layer thickness is controlled by the plate geometry. Conditions at which the web touches the plate can still by estimated by using threshold limits in the air-layer thickness.

Solution method

The governing equations and the boundary conditions, Eqs. 3 to 5, give rise to a *free-boundary problem*. The location of the web is unknown *a priori*. The basis of treating such problems is briefly recounted here. Fuller accounts were given by Kistler and Scriven (1983, 1984) and Sackinger et al. (1996).

In order to solve a free-boundary problem using standard techniques for boundary-value problems, the set of differential equations posed in the unknown physical domain has to be transformed to an equivalent set defined in a known, fixed-reference domain. This approach has been extensively used to solve viscous flow with liquid/air interface (see Kistler and Scriven, 1983). In that class of problem, the position of the liquid/air interface is implicitly located by imposing the kinematic boundary condition at the interface. In the situation studied here, the position of the web is implicitly located by imposing the system of ordinary differential equations (Eqs. 4).

The transformation of the set of differential equations that governs the problem is made by a mapping $\boldsymbol{x} = \boldsymbol{x}(\xi)$ that connects the physical domain, parameterized by the position vector $\boldsymbol{x}$, and reference domain, parameterized by ξ. The inverse of the mapping $\boldsymbol{x} = \boldsymbol{x}(\xi)$ is governed by a pair of elliptic differential equations identical with those encountered in the dilute regime of diffusional transport. The coordinate potentials ξ and η satisfy

$$\nabla\cdot\left(D_\xi\nabla_\xi\right) = 0 \quad \text{and} \quad \nabla\cdot\left(D_\eta\nabla_\eta\right) = 0 \tag{6}$$

where D_ξ and D_η are the diffusion coefficients. They control the spacing of the curves of constant ξ and η chosen to tessellate the domain.

The Navier–Stokes (Eqs. 3), the substrate deformation (Eqs. 4), and the mesh generation equations (Eqs. 6), together with the respective boundary conditions were solved by the Galerkin/finite-element method. Biquadratic basis functions were used to represent both the velocity and the mapping from the reference to the physical domain. The basis functions used to represent the pressure field were piecewise, linear, and discontinuous.

The resulting nonlinear system of algebraic equations for the coefficients of the basis functions were solved by Newton's method. The domain was divided into 476 elements with 8,928 unknowns. The computations were performed in a HP model J-200 workstation, and each solution took approximately 10 min to compute. Figure 6 shows a representative mesh with $Y < 0$.

In order to obtain solutions at large wrapping angles, that is, large values of Y, a good initial guess is vital. The procedure adopted was to first obtain solutions with the plate far from the web, that is, $Y < 0$. At these conditions, the pressure that builds up in the air is very small, leading to small web deformation. A solution can be obtained even with a poor initial guess. After a solution is computed, a first-order, arc-length continuation on the position of the plate was used to obtain solutions at the relevant set of parameters. Figure 7 illustrates a sequence of solutions as the plate is moved upwards and pushed against the web.

Figure 6. Representative mesh used to discretize the problem: 476 elements and 8,929 unknowns.

Theoretical Predictions

As mentioned before, both the coordinate of the middle point of the plate Y or the position S^* of the point where the

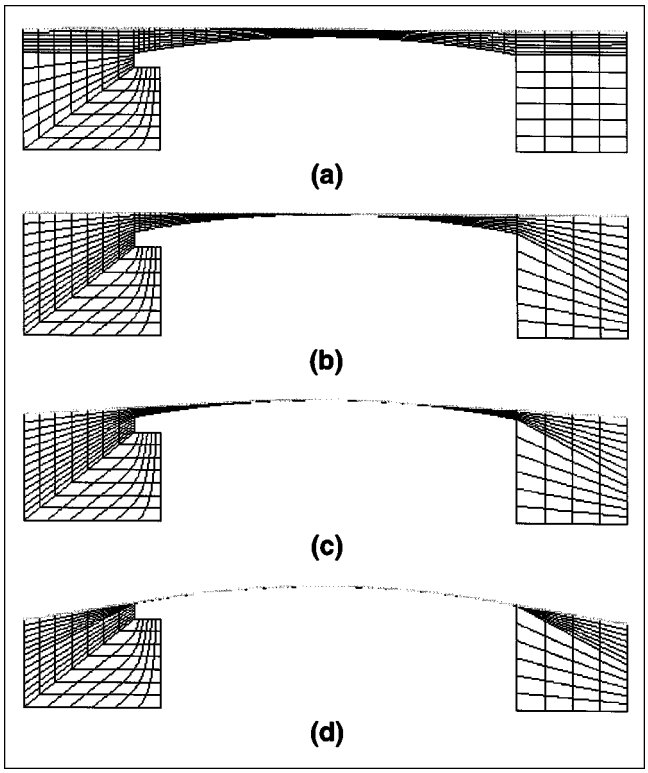

Figure 7. Sequence of solutions as the plate is pushed against the moving web.

$R_0 = 24.4$ m; $L = 1.52$ m; and (a) $Y = -0.508$ cm; (b) $Y = 0.0$ cm; (c) $Y = 1.016$ cm; and (d) $Y = 2.286$ cm.

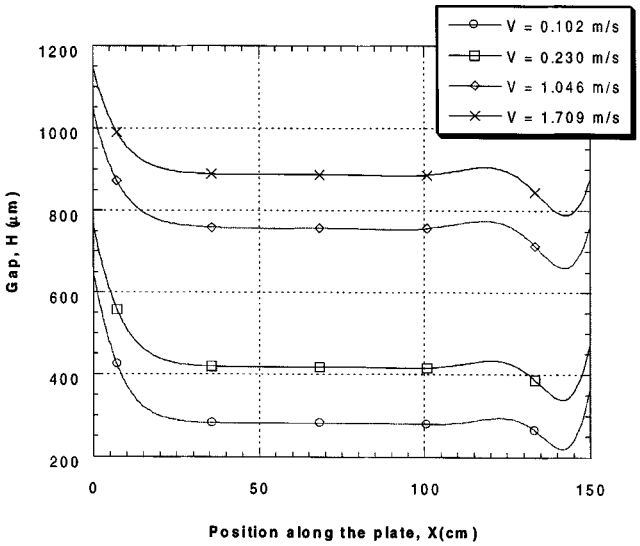

Figure 8. Clearance between the web and Plate 1 at different web speeds (tension number).

$S^* = 12.7$ cm; $T = 0.1$ kg/cm; and $N_{ES} = 1.6\times10^{-11}$.

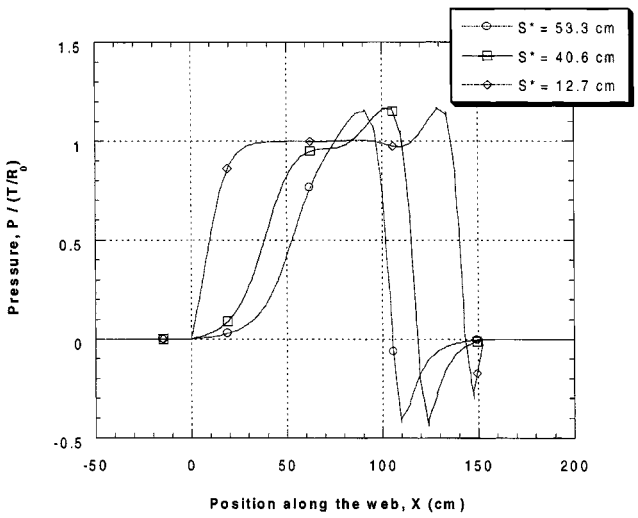

Figure 10. Pressure distribution along the substrate moving over Plate 1 at $\tau = 2\times10^{-8}$ and $N_{ES} = 1.6\times10^{-11}$.

web first touches the plate, when it is stationary, can be used to characterize the relative position of the plate and the idlers that guide the substrate. The latter is easier to measure experimentally, and for this reason is used here.

Base case

As a base for comparison, the theoretical predictions obtained for a web traveling over a plate 1.52 m (5 ft) long with a radius of curvature equal to 24.4 m (80 ft) are presented first. As a matter of reference, this configuration is called *Plate 1*. Figure 8 illustrates the gap between the web and the plate at different web speeds, at a tension of $T = 0.1$ kg/cm (0.6 lb/in.)–Tension number τ from 2×10^{-8} up to 3.4×10^{-7}. The position of the plate was fixed at $S^* = 12.7$ cm, and the Elasticity number at $N_{ES} = 1.6\times10^{-11}$. The flow can be divided into three regions. The first one is the inflow, where the web approaches the plate. Next, is a region of more or less constant clearance H_0. The last portion, the outflow region, is characterized by an undulation of the web. The minimum gap between the web and the plate $H_{\min}$ occurs close to the end of the plate. For the purpose of determining the heat transfer from the hot plate to the web, the relevant dimension is the almost constant clearance H_0. As the web speed increases, more air is dragged by the moving substrate, raising the clearance, H_0.

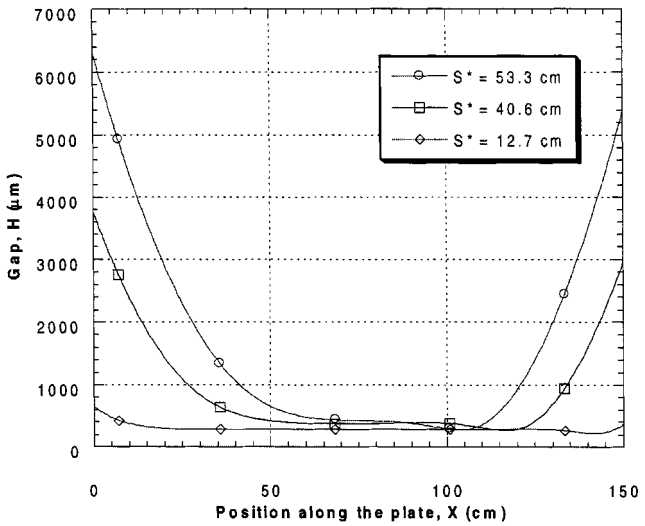

Figure 9. Clearance between the web and Plate 1 at different tangent point position.

$\tau = 2\times10^{-8}$ ($V = 0.102$ m/s and $T = 0.1$ kg/cm) and $N_{ES} = 1.6\times10^{-11}$.

The effect of the position of the plate, represented by S^*, on the clearance between the web and the plate is illustrated in Figure 9. The Tension number is $\tau = 2\times10^{-8}$, which corresponds to a line tension $T = 0.1$ kg/cm and web speed $V = 0.102$ m/s, and the Elasticity number is $N_{ES} = 1.6\times10^{-11}$. As the tangent point approaches the upstream edge of the plate, that is, as S^* falls, the region of uniform gap is extended, completely separating the inflow from the outflow region, and the air-layer thickness decreases.

The converging channel at the inflow region leads to a pressure buildup in the flowing air, as illustrated in Figure 10. In the uniform gap region, the pressure is almost constant and approximately equal to the tension applied to the web divided by the radius of curvature of the plate, or $P \approx T/R_0$. There is a pure Couette flow. In this class of flow, the channel height is linearly proportional to the flow rate dragged by the web. If there is no leakage, the flow rate is controlled by the two-dimensional flow in the entrance region. There, the flow is approximately one-dimensional and is well described by a combination of Couette and Poiseuille flow. With this approximation, it follows from elastohydrodynamic theory that the maximum pressure gradient is inversely proportional to the square of the flow rate. The larger the pressure gradi-

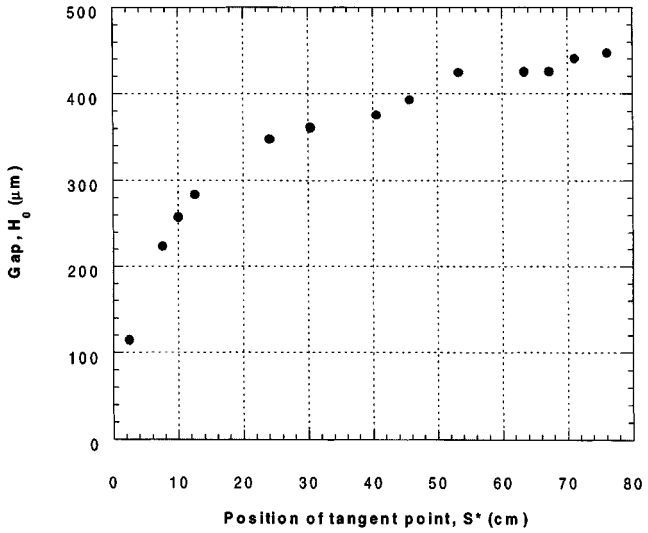

Figure 11. Variation of gap between the substrate and Plate 1 at different tangent point position S^*: $\tau = 2\times10^{-8}$ and $N_{ES} = 1.6\times10^{-11}$.

ent in the inlet region, the more air is rejected and the smaller the flow rate through the gap. As S^* falls, the uniform pressure region is extended closer to the edge of the plate and the adverse pressure gradient at the inlet increases, leading to a smaller air flow rate, and consequentially a smaller float height, as shown in Figure 10.

Figure 11 summarizes the effect of the relative position of the plate and idlers (measured by S^*) at a Tension number $\tau = 2\times10^{-8}$ and Elasticity number $N_{ES} = 1.6\times10^{-11}$. At $S^* = 76.2$ cm, $Y = 0$ and the web is tangent to the plate at its middle point M. The graph can be divided into three distinct regions. The first region corresponds to the transition from a tangent web to one that is wrapped around part of the curved surface of the plate. The clearance H_0 falls slightly (from approximately 450 μm to 420 μm). In the second region, the effect of the position of the tangent point on the gap between the web and the plate is small: H_0 varies from 420 μm to 350 μm, as S^* varies from 70 cm to 25 cm. As the plate is pushed further against the web, and S^* decreases even more, the flow is strongly affected by the position of the tangent point. The float height can be reduced from 350 μm to 120 μm as the tangent point moves from 25 cm to 5 cm away from the edge of the plate.

In a gap dryer, the upstream idler has to be adjusted such that the tangent point is close to the leading edge of the plate in order to take advantage of the entire length of the heated plate to increase the web temperature. It is clear from Figure 11 that, in such condition, the position of the substrate is critical to the value of the clearance between the moving web and the curved plate. Moreover, the Knox–Sweeney equation cannot be accurately used to estimate the air-layer thickness. At the conditions of the predictions shown in Figure 11, the Knox–Sweeney equation estimates an air-layer thickness of 390 μm.

In the range of parameters explored in this work, the clearance between the substrate and the curved plate did not vary with the Elasticity number. It is important to notice that Eshel and Elrod (1967) have shown that the stiffness of the web

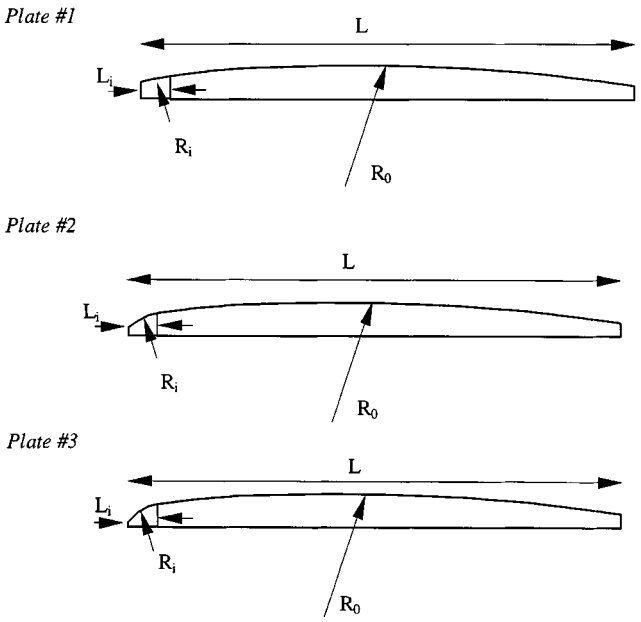

Figure 12. Sketch of plates with different entrance regions.

All plates are 1.52 m long with main radius of curvature of $R_0 = 24.4$ m. The entry section is 10.16 cm long.

D decreases the air-layer thickness. However, their work was related with magnetic tape floating over read–write heads that have a radius of curvature much smaller than those explored here. From asymptotic analysis, it can be shown that the Elasticity number is only relevant to the problem when it is in the same order of magnitude as the Tension number to the power 2/3 that is

$$\frac{D}{TR_0^2} \approx O\left[\left(\frac{\mu V}{T}\right)^{2/3}\right]$$

This condition is not satisfied in the situations explored in this work.

Effect of the geometry of the leading edge of the plate

From the results presented in the previous subsection, it is clear that the float height can be modified by controlling the pressure gradient at the leading edge of the plate. One way of accomplishing that is to change the position S^* at which the web approaches the plate, as illustrated in Figure 11. This alternative is not always possible, since changes on the position at which the web approaches the plate may alter the overall web path on an existing coating line.

An alternative way is to change the geometry of the leading edge of the radius plate. This alternative is explored in this section by studying the float height of a web traveling over three different plates. Figure 12 illustrates the main geometric parameters of the plates analyzed here. They all had a length of $L = 1.52$ m (5 ft) and a main radius of curvature of $R_0 = 24.4$ m (80 ft). The only difference between them was the geometry of the entry section, where the web first approaches the plate (the web is moving from left to right in the figure). The entry sections of all the plates were 10.2 cm long

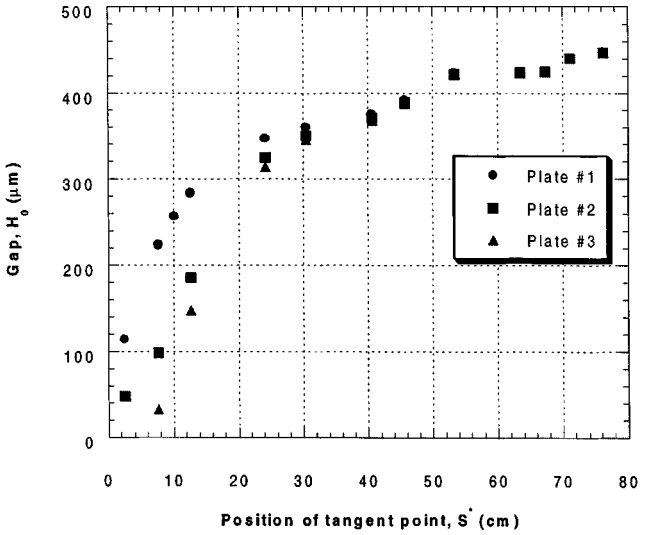

Figure 13. Variation of air-layer thickness between web and Plates 1, 2, and 3 at different tangent point positions S^*.

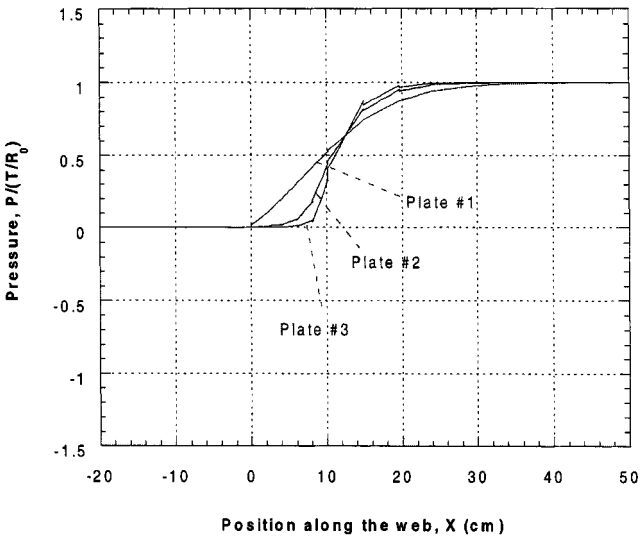

Figure 15. Pressure distribution along the web at the conditions shown in Figure 14.

and also curved. Plate 1 had an entry radius equal to the rest of the plate, that is, $R_i = 24.4$ m (80 ft) (this is the geometry analyzed as a base case in the previous section). Plate 2 had an entry radius equal to $R_i = 1.52$ m (5 ft), and Plate 3 had an entry radius equal to $R_i = 0.6$ m (2 ft). The transition between the entry section and the rest of the plate was smooth, that is, the curved surfaces were tangent at the point (line in 3-D) where they met.

Figure 13 shows how the clearance between the web and the plate varies with the tangent point for the three different plates. The results of Plate 1 were already presented in Figure 11. At large values of S^*, the flow is not affected by the configuration of the entrance region and the predictions of all three plates are virtually the same. As the plate is pushed against the web, and S^* falls, the flow starts to be affected by the geometry of the upstream edge of the plate. At $S^* \leq 25.4$ cm, the float height is strongly dependent not only on the tangent point but also on the geometry of the entry section. At a fixed value of S^*, the clearance was maximum with Plate 1 and minimum with Plate 3. At $S^* = 12.7$ cm, the float height obtained with Plate 3 is close to half of that obtained with Plate 1.

Figures 14 and 15 show the gap profile and the pressure along the web for the three plates at Tension number $\tau = 2 \times 10^{-8}$, Elasticity number $N_{ES} = 1.6 \times 10^{-11}$, and $S^* = 12.7$ cm. The middle part of the flow is characterized by the almost constant clearance channel formed between the web and the plate. The pressure in this region is virtually constant and close to the ratio between the web tension and the radius of the plate, $P \approx T/R_0$. Although the pressure along most of the plate is the same for all three geometries, the pressure gradient at the inflow region is quite different, as illustrated in Figure 15, leading to the difference on float height. As expected, the largest adverse pressure gradient (Plate 3) leads to the smallest float height (see Figure 15).

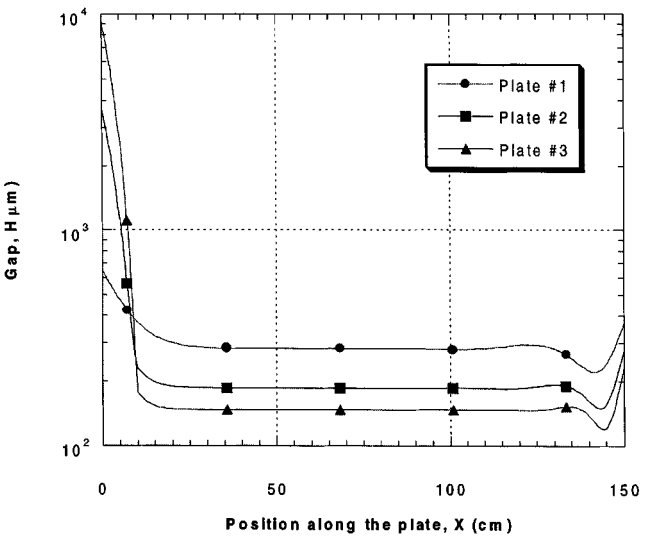

Figure 14. Gap between the moving substrate and Plates 1, 2, and 3: $\tau = 2 \times 10^{-8}$ and $N_{ES} = 1.6 \times 10^{-11}$.

The effect of web speed or line tension (through the Tension number τ) on the air-layer thickness for the three different plates is shown in Figure 16, at Elasticity number $N_{ES} = 1.6 \times 10^{-11}$ and $S^* = 12.7$ cm. The predictions of the Knox–Sweeney equation are also plotted. As expected, the float height increases as the Tension number rises (higher web speed or lower web tension) for all plates. At the range of Tension number explored, Plate 1 yielded the highest float height. However, the effect of the entry-section geometry diminishes as the web speed increases. It is important to note that the Knox–Sweeney equation overpredicts the float height by a factor as high as 3, and cannot be accurately used to estimate air-layer thickness.

Effect of weight of substrate

In all the results presented up to this point, the weight of the substrate was neglected. Because the theoretical predic-

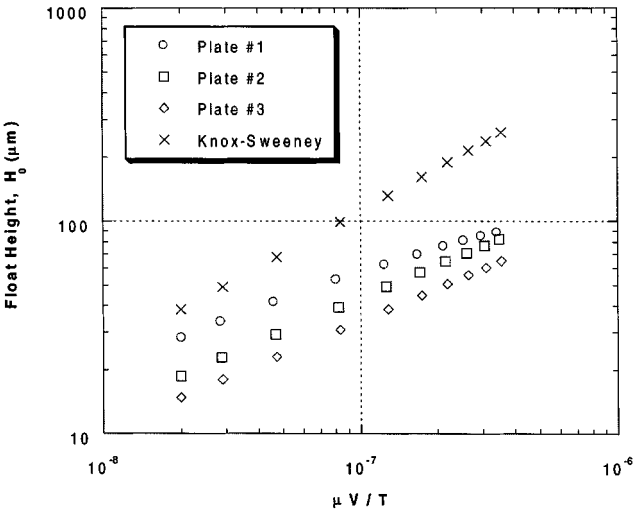

Figure 16. Comparison of gap as a function of Tension number $\tau \equiv \mu V/T$ for Plates 1, 2, 3, and the Knox–Sweeney equation.

tions were insensitive to the web stiffness, the air-layer thickness did not vary with the film caliper. However, experimental measurements, shown in the following section, show that at some operating conditions, the higher the film caliper, the smaller the clearance between the web and the curved plate. This subsection shows that the substrate caliper affects the air-layer thickness because the gap between the web and plate depends on the Weight number $W \equiv \rho_w gtL_i/T$.

The boundary conditions used for the curvature equation along the deformable substrate (4-b) in the cases at which the weight of the web was not neglected were the same ones used in the case of the vanishing Weight number, that is, zero curvature at both ends of the tensioned web. When the weight of the substrate is taken into account, this boundary condition is an approximation of the real situation. The substrate bends in the free span between the idler rolls and the plate, and the curvature at the points where the substrate touches the rolls is different than zero. However, the effect of the curvature at the boundaries of the domain of calculation of the substrate is restricted to a region close to the boundaries and decays exponentially. The nonzero curvature at the idler rolls has negligible effect on the shape of the substrate near the plate and therefore on the entrained air-layer thickness.

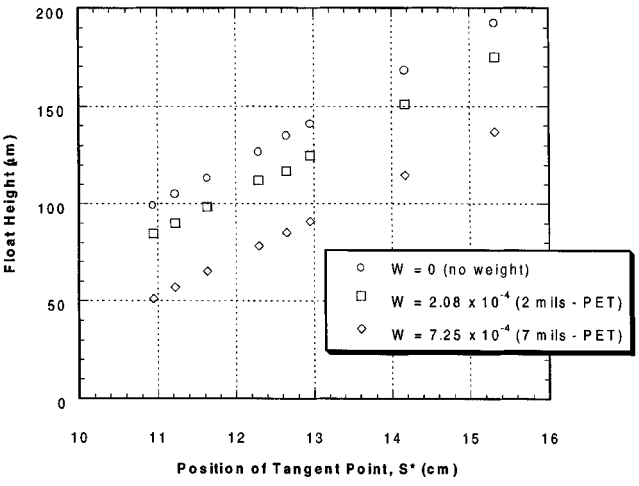

Figure 17. Effect of Weight number on the air-layer thickness.

Figure 17 shows the air-layer thickness at a web speed of $V = 0.255$ m/s, and $W = 0$ (substrate with no weight), $W = 2.08 \times 10^{-4}$ [corresponds to a 50.8-μm (2-mil) PET web, running with a tension of $T = 0.22$ kg/cm (1.2 lb/in.) and with an upstream idler $L_i = 6.35$ cm away from the front edge of the plate], and $W = 7.25 \times 10^{-4}$ [corresponds to a 177.8-μm (7-mil) PET web, running with a tension of $T = 0.22$ kg/cm (1.2 lb/in.) and with an upstream idler $L_i = 6.35$ cm away from the front edge of the plate]. At a given set of operating conditions, the predicted clearance decreases with web thickness.

The weight of the moving substrate can affect the air-layer thickness through two different mechanisms. The weight counteracts the force due to the air pressure between the web and the curved plate (see Figure 5), tending to reduce the clearance between the surfaces. The second mechanism is that the web bends downward, due to its weight in the free span between the upstream idler roll and the plate, altering the geometry of the entry section that defines the air flow rate and therefore the air-layer thickness. A simple order-of-magnitude analysis shows that the effect of the first mechanism is negligible, the air pressure underneath the web is orders of magnitude larger than the substrate weight. The second mechanism is the one responsible for the reduction of the air-layer thickness with the weight of the web. Because the web bends, the tangent point, where the stationary web first touches the plate is shifted upstream, closer to the front edge of the plate, leading to a smaller air-layer thickness.

The air-layer thickness, including the effect of substrate weight, can be estimated from the predictions obtained with $W = 0$. The idea is to estimate a shift in the tangent point position ΔS^* due to the bending of the web on the free span. This can be done using simple geometric arguments. The shift in the position of the tangent point can be approximated in terms of the free span between the upstream idler and the plate $l = L_i + S^*$, plate radius R_0, line tension T, web density ρ_w and thickness t, and the angle α between the x-axis (along which S^* is measured) and the horizontal direction

$$\Delta S^* = \frac{\frac{l}{2}}{1 + \frac{\sqrt{(T/\rho_w tg\ \cos\ \alpha)^2 + (l/2)^2}}{R_0}} \approx \frac{l/2}{1 + \frac{T}{\rho_w tgR_0\ \cos\ \alpha}}$$

If the theoretical predictions presented in Figure 17 are plotted as a function of the modified tangent-point position that takes into account the bending of the web, that is, $S^*_{\text{mod}} = S^* - \Delta S^*$, the computed air-layer thickness for three different weight numbers almost coincide, as illustrated in Figure 18. The small variation observed is attributed to the oversimplified analysis for determining ΔS^*. The main conclusion from Figure 18 is that for a given plate, the air-layer thickness can be expressed as a function of a modified tangent point $S^*_{\text{mod}} = S^* - \Delta S^*$ and the tension number τ. The effect of the web thickness and density, that is, its weight, can be incorporated in the correction term ΔS^*.

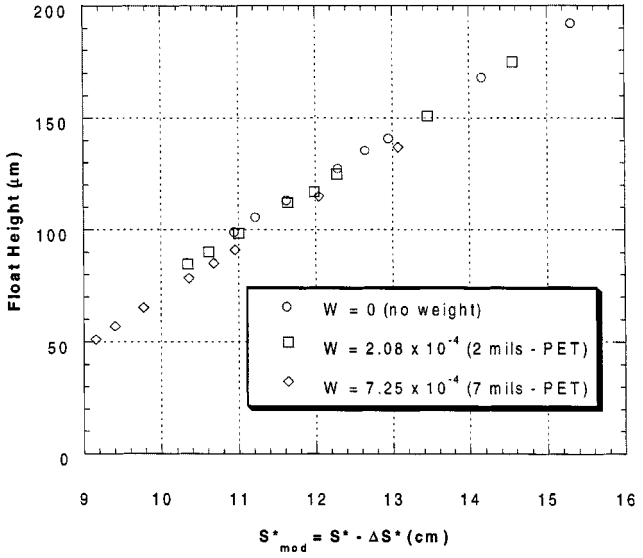

Figure 18. Air-layer thickness as a function of the modified tangent point position S^*_{mod}.

The curves at different Weight numbers almost coincide.

Experimental Analysis

The goals of the experimental analysis were to validate the accuracy of the theoretical model and to study the issues not accounted for in the model, such as air leakage through the sides and variation of the air-layer thickness in the transverse direction.

The experiments consisted of measuring the distance between the moving substrate and the curved plate at different locations and at different operating conditions.

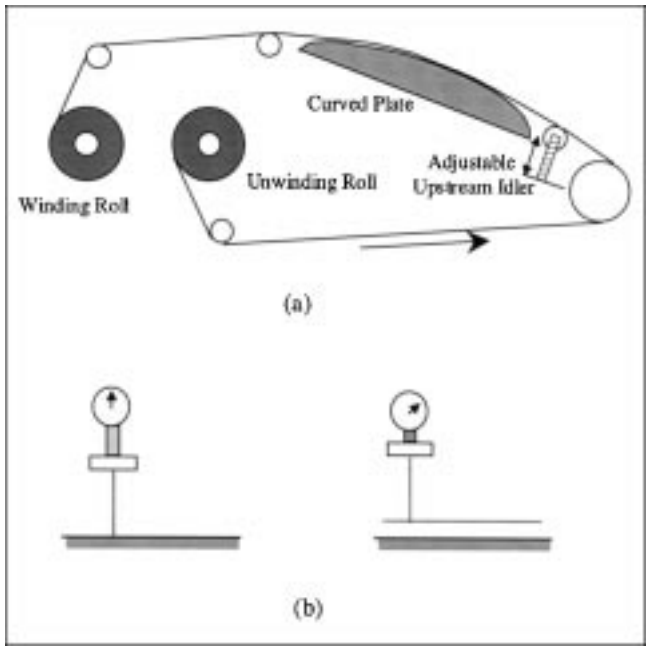

Figure 19. Experimental apparatus.

(a) Web line with curved plate and adjustable upstream idler; (b) technique for air-layer thickness measurement.

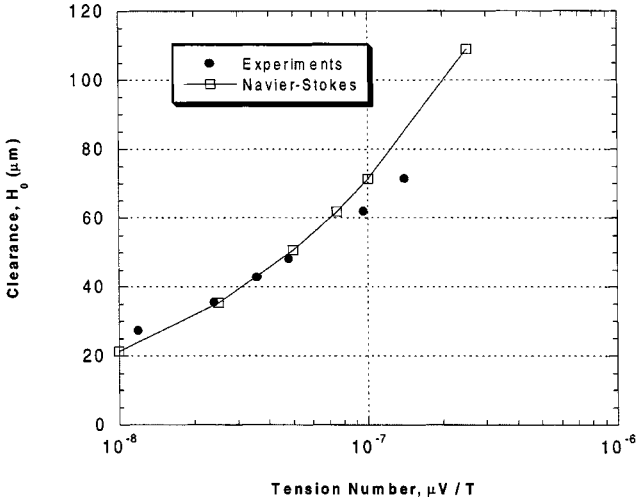

Figure 20. Experimental measurements vs. air-layer thickness predictions at different Tension number τ and $S^* = 24.6$ cm.

Experimental setup

The experimental setup is sketched in Figure 19. It consisted of winding and unwinding stations to supply and collect the substrate, an adjustable upstream idler to control the position of the moving web relative to the plate, and a radius plate with a geometric configuration identical to Plate 3 used in the theoretical predictions. The velocity and tension of the substrate over the plate were independently controlled. The relative position of the web to the plate was measured by the location of the point at which the tensioned and stationary substrate would first touch the plate if it were straight. In reality, the web bends from its own weight. To eliminate the effect of the weight of the substrate on this parameter, the tangent point location was obtained using a ruler sitting on the upstream idler and the radius plate.

At each set of operating conditions, that is, velocity, tension, and position of the upstream idler, the distance between the moving web and the plate was obtained at different locations over the plate, both cross-web and down-web. The air-layer thickness was measured with a micrometer attached to a sliding needle. The needle was first pushed against the plate (without the substrate in between them). At that position, the micrometer scale was set to zero. Then, the needle was moved away from the plate, and the substrate was placed over the plate and under the needle, ready for operation. At each condition, the needle was slowly brought closer to the plate, until it touched the substrate. The micrometer reading minus the caliper of the substrate corresponded to the air-layer thickness. In order to accurately establish if the needle had touched the web, a video camera with magnifying lenses was used to enhance the view of the area close the tip of the needle.

Results

The effect of tension number on the measured air-layer thickness is shown in Figure 20. The web velocity varied from 0.102 m/s to 1.53 m/s and the tension was fixed at 0.2 kg/cm (1.1 lb/in.) on a substrate 22.5 cm (9 in.) wide, leading to a

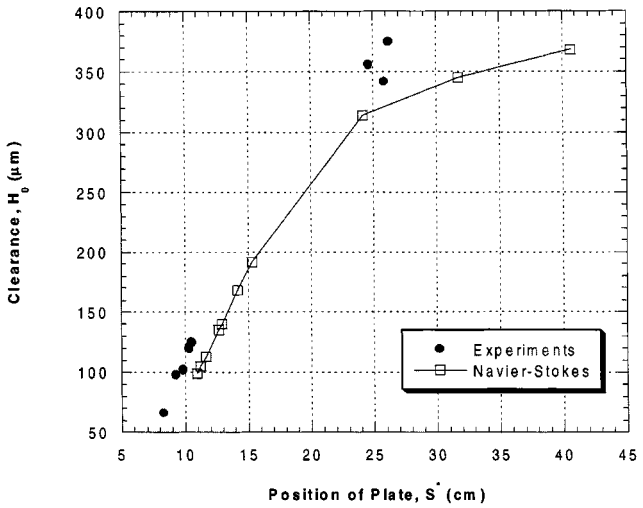

Figure 21. Experimental measurements vs. air-layer thickness predictions at different tangent-point position and Tension number $\tau = 2.4 \times 10^{-8}$.

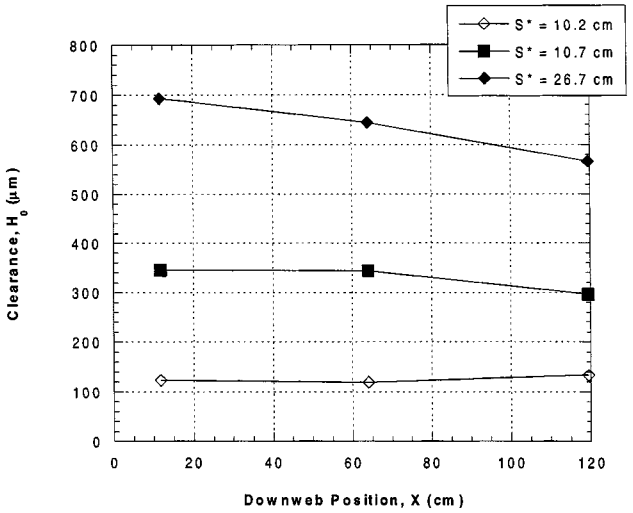

Figure 23. Downweb variation of air-layer thickness at Tension number $\tau = 9.6 \times 10^{-8}$ and $S^* =$ 10.2, 10.7 and 26.7 cm.

variation on tension number from 1.2×10^{-8} to 1.45×10^{-7}. The tangent-point location was fixed at $S^* = 24.6$ cm. As expected, the air-layer thickness increases with web speed. The faster the substrate, the more air it entrains, increasing the clearance between the two surfaces. The plot also shows the theoretical predictions at the same conditions. The agreement over the entire range of tension number was very good, especially at low clearance. At larger air-layer thicknesses, the amount of air that leaks through the sides is not negligible, is shown in the following discussion, which accounts for the smaller measured air-layer thickness.

Figure 21 compares the measured air-layer thickness with the theoretical predictions at $\tau \equiv \mu V/T = 2.4 \times 10^{-8}$ and different tangent-point positions. The agreement is again very good over the entire range.

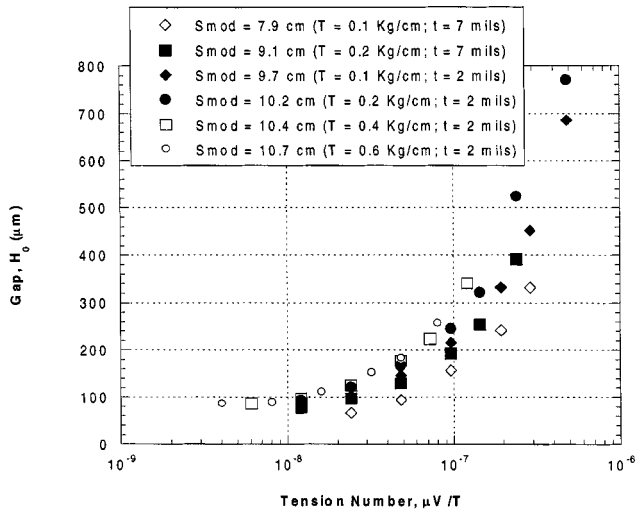

Figure 22. Measured air-layer thickness at $S^* = 10.8$ cm, and different web speed, tension, and density.

The gap is a function of the modified tangent-point location, S^*_{mod}.

The effect of the substrate weight was also analyzed experimentally. The air-layer thickness at different tension numbers was measured for two different webs (thickness of 50.8 and 172.7 μm; i.e., 2 and 7 mil) at different line tensions, and upstream idler position fixed at $S^* = 10.8$ cm. The modified tangent point S^*_{mod}, defined in the previous section, is different for each condition analyzed. The correction for the tangent-point position ΔS^* due to its own bending over the free span rises as the substrate caliper increases and the line tension decreases. Figure 22 shows the measured clearance. It can be observed that for a given tension number, $\tau \equiv \mu V/T$, the air-layer thickness increases with S^*_{mod}, as predicted by the theoretical model. The effect of weight can be large: at $\mu V/T = 10^{-7}$, the clearance with a 2-mil web and line tension $T = 0.6$ kg/cm is twice the one obtained with a 7-mil web and line tension $T = 0.1$ kg/cm.

It is clear that the theoretical model presented here is able to capture the main physics that governs this situation. The air-layer thickness predictions agree well with the measurements. However, the measurements are not only used to validate the accuracy of the prediction, but also to analyze the limits of the assumption made in the theoretical model that there is no air leakage from underneath the substrate. This was done by looking at the air-layer thickness at different positions along and across the plate.

Figure 23 shows the variation of the air-layer thickness along the length of the plate at tangent-point positions equal to $S^* = 10.2$, 10.7 and 26.7 cm. The tension number was $\tau \equiv 9.6 \times 10^{-8}$. At small clearances, air leakage is very small. When the air-layer thickness is close to 125 μm, the clearance between the moving web and the plate is virtually constant along the plate. At larger gaps, air escapes from underneath the substrate, and the clearance decreases as the web travels along the length of the plate. The virtually vanishing leakage at small clearances can be easily explained by Figure 24. It shows the air-layer thickness profile across the web at a

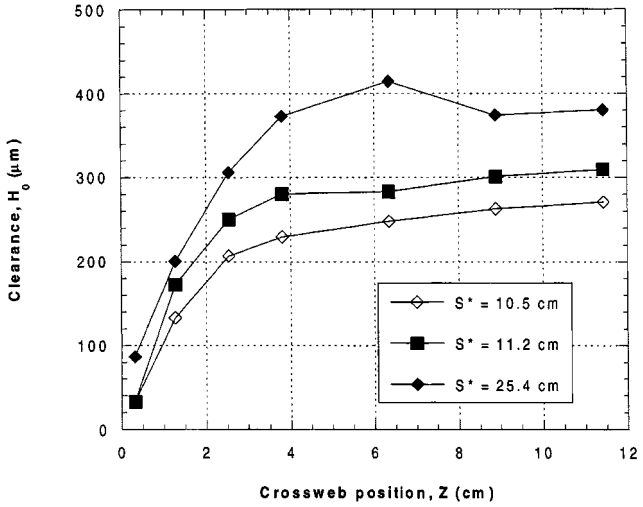

Figure 24. Crossweb variation of air-layer thickness at $\tau = 9.6\times10^{-8}$ and $S^* = 10.5$, 11.2 and 25.4 cm.

tangent-point position equal to $S^* = 10.5$, 11.2, and 25.4 cm. The tension number was again $\tau \equiv 9.6\times10^{-8}$. Close to the edges of the substrate, the clearance is much smaller than in the middle, and the air is to some degree sealed between the two surfaces. At small clearances, this effect is stronger, the gap on the sides of the web is very small, and the air is almost completely sealed between the substrate and the plate. In these situations, the cross-web variation of the air-layer thickness is limited to approximately 2.5 cm in each side of the substrate. At larger air-layer thicknesses, for example, close to 400 μm, the clearance profile is not so uniform and the gap at the sides of the web is large enough that some of the air can escape from underneath the substrate.

These results show that the two-dimensional model used here is adequate to study air flow between moving web and curved plate at the range of parameters of interest for gap drying application, where the usual target air-layer thickness is from 75 μm to 250 μm.

Final Remarks

For an efficient utilization of the *gap drying* technology (Huelsman and Kolb, 1997), it is important to control the clearance between the moving substrate and the curved heated plate. Moreover, because the same coating line can be used for different products that have different drying requirements, it is important to be able to easily change the air-layer thickness between the two surfaces in order to adjust the heat-transfer coefficient. The theoretical and experimental analyses presented here clarified the mechanisms related with this elastohydrodynamic situation. They showed that the clearance between the two surfaces is controlled by the pressure gradient at the entrance section of the channel formed between the web and the plate.

Based on the understanding of the flow, different ways of controlling the clearance between a moving web and a curved plate are discussed next (see Figure 25).

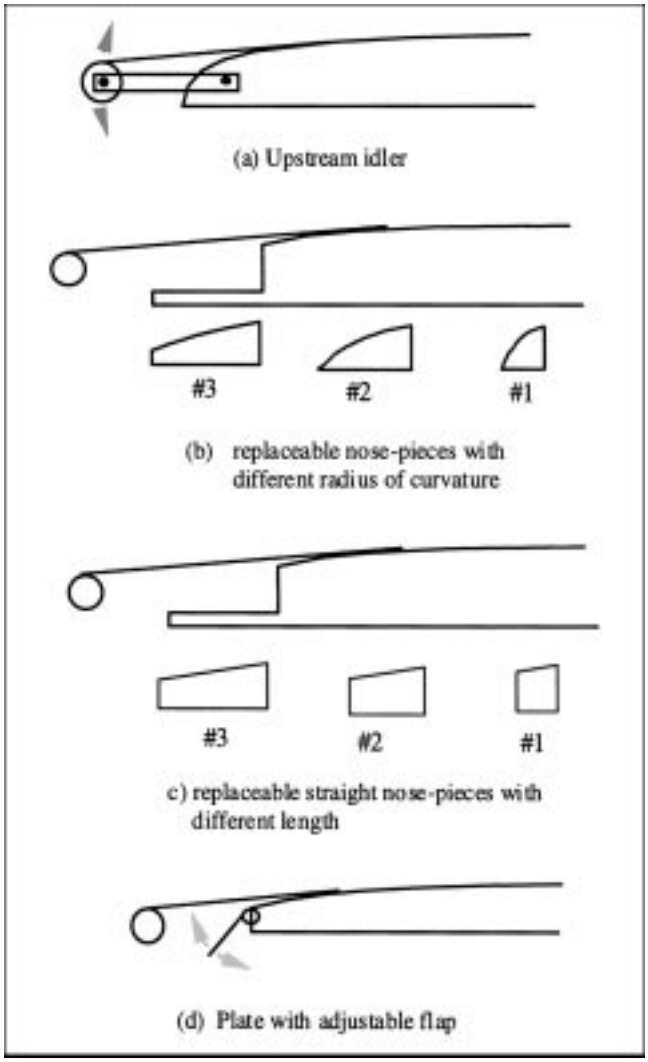

Figure 25. Different configurations for controlling the air-layer thickness.

• *Upstream Idler Roll*. An idler roll installed just upstream from the plate can be used to change the position of the tangent point, S^*. As previously discussed, this alternative continuously covers a very wide range of clearances. The limitation of this method is that it cannot be used between plates in a multizones oven, since the position of the idler would affect the plates located upstream of it.

• *Nose Pieces*. A way of changing the pressure gradient without moving the tangent point is to use different geometries on the front edge of the plate. One possible choice is to have nose pieces, each with a different radius of curvature, as in the analysis presented before. In Figure 25, Piece 1 would give the smallest air-layer thickness, the Piece 3, the largest. Another possible situation is to have straight nose-pieces of different lengths. A limitation of this method is that it gives a discrete adjustment of air-layer thickness.

• *Flaps*. Instead of adjusting the geometry of the entry section by removable pieces, another option is to use a flap that

can have its angle changed with respect to the plate, as sketched in Figure 25. The clearance falls as the flap angle approaches the vertical position.

Literature Cited

Blok, H., and J. J. van Rossum, "The Foil Bearing: A New Departure in Hydrodynamic Lubrication," *Lubr. Eng.*, **9**, 316 (1953).

Eshel, A., and H. G. Elrod, "The Theory of Infinitely Wide, Perfectly Flexible, Self-Acting Foil Bearing," *J. Basic Eng.*, **87**, 831 (1965).

Eshel, A., and H. G. Elrod, "Stiffness Effects on the Infinitely Wide Foil Bearing," *J. Lub. Technol.*, **89**, 92 (1967).

Eshel, A., "On Controlling the Film Thickness in Self-Acting Foil Bearings," *J. Lubr. Technol.*, **92**, 359 (1970).

Huelsman, G. L., and W. B. Kolb, "Coated Substrate Drying System," U.S. Patent No. 5,694,701, Minnesota Mining and Manufacturing Company (1997).

Kistler, S. F., and L. E. Scriven, "Coating Flows," *Computational Analysis of Polymer Processing*, J. R. A. Pearson and S. M. Richardson, eds. Applied Science Publishers, London (1983).

Kistler, S. F., and L. E. Scriven, "Coating Flow Theory by Finite Element and Asymptotic Analysis of the Navier-Stokes System," *Int. J. Numer. Methods Fluids*, **4**, 207 (1984).

Knox, L. K., and T. L. Sweeney, "Fluid Effects Associated with Web Handling," *Ind. Chem. Process Design Dev.*, **10**, 201 (1971).

Kolb, W. B., and G. L. Huelsman, "Gap Drying: An Overview," *Int. Coating Science and Technology Symp.*, published by University of Minnesota, p. 209 (1998).

Licht, L., "An Experimental Study of Elastohydrodynamic Lubrication of Foil Bearings," *J. Lub. Technol.*, **90**, 199 (1968).

Sakinger, P. A., P. R. Schunk, and R. R. Rao, "A Newton-Raphson Pseudo-Solid Domain Mapping Technique for Free and Moving Boundary Problems: A Finite Element Implementation," *J. Comput. Phys.*, **125**, 83 (1996).

Manuscript received April 13, 2000, and revision received Oct. 5, 2001.